Journal of Crystal Growth 390 (2014) 92–95

Contents lists available at ScienceDirect

Journal of Crystal Growth

journal homepage: www.elsevier.com/locate/jcrysgro

Solid solution strengthening and phase transformation in high-temperature annealed $Si_{80}Ge_{20}$ alloy

Tun-Yuan Chiang [a,1], Hua-Chiang Wen [b,1], Wu-Ching Chou [b], Chien-Huang Tsai [c,*]

[a] Department of Mechanical Engineering, Chin-Yi University of Technology, Taichung 400, Taiwan, ROC
[b] Department of Electrophysics, National Chiao Tung University, Hsinchu 300, Taiwan, ROC
[c] Department of Automation Engineering, Nan Kai University of Techonology, No. 568, Zhongzheng Road, Caotun Township, Nantou 54243, Taiwan, ROC

ARTICLE INFO

Article history:
Received 3 August 2013
Received in revised form
20 October 2013
Accepted 10 December 2013
Communicated by A.G. Ostrogorsky
Available online 22 December 2013

Keywords:
A1. Characterization
A1. Crystal structure
B2. Semiconducting silicon compounds

ABSTRACT

This investigation demonstrates the temperature-dependent mechanical properties of $Si_{80}Ge_{20}$ alloy films via a nanoindenter in the indentation depth of 100 nm. The roughly equal root mean square roughness (R_{rms}) values and repeatable load–displacement (P–δ) curves for the samples ensure the mechanical performances mainly contributed from the influences of annealing temperatures. The hardness (H) values of samples increase with the temperatures of an initial annealing in the range from RT to 900 °C, and, conversely, decrease for annealing temperatures over 900 °C. Accordingly, both E/H and h_f/h_{max} values, exhibiting an inverse tendency in the above temperature range, hints that the solid solution strengthening effect and the softening phenomenon occur for the initial-annealing and over-annealing stages, respectively. In addition, grazing incidence X-ray diffraction (GIXRD) analysis demonstrates the lattice expansion and the broadened peak that attribute to the solid solution strengthening of samples and the segregation of Ge, respectively. Through observing the value of the (200) lattice spacing of 5.624 Å for a 900 °C-annealed sample by transmission electron microscopy (TEM) analysis, it is verified that the segregation of Ge is responsible for the decreased hardness for the 1000 °C-annealed sample.

1. Introduction

Given several attractive features including tunable band gaps, high carrier densities, a complete solid solution character, and high thermal conductivity, silicon–germanium (Si–Ge) alloys are considered as potential materials for the applications for solar cells [1], photodetectors [2], light-emitting diodes [3], integrated optical [4] and photovoltaic [5] devices, heterojunctions [6], one-dimensional devices [7], standard resistors [8], and single-grain thin-film transistors [9]. Owing to the high quality of thin films, an ultrahigh-vacuum chemical deposition (UHV-CVD) is one of the popular procedures for the fabrication of Si–Ge films. Because of a thermal dissociation of precursors (e.g., silane and germane) and rapid deposition, UHV-CVD yielded metastable defects, and many researchers made efforts to overcome this problem. Kringhøj et al. [10] relaxed the lattice strain of the $Si_{0.915}Ge_{0.085}$ alloy film by annealing samples at 1100 °C. Parnis et al. [11] averaged magnitudes of fluctuations of X-ray diffraction spectra using a novel simulation procedure, and quantitatively characterized the degree of a structural disorder for the $Si_{0.78}Ge_{0.22}$ film. For the $Si_{0.5}Ge_{0.5}$ film, Whiteaker et al. [12] showed an increase of the averaged order parameter with increasing thickness, but then a decrease with the thickest film of 1000 Å. These features elucidate the importance of the phase- and the defect- controls for ultra-thin Si–Ge alloy films. Except for the physical properties mentioned above, the mechanical performances for Si–Ge films are also influenced from the micro- or nano-scaled imperfections. Under the annealing treatments from RT to 1000 °C, this study seeks to investigate the effects of detailed structural transformations on mechanical behaviors of a $Si_{80}Ge_{20}$ film. Predictably, the mechanism of mechanical variations could be inferred via a grazing incidence X-ray diffraction (GIXRD) and transmission electron microscopy (TEM).

2. Experimental details

An ultra-high vacuum chemical vapor deposition (UHV-CVD) system was applied for depositing Si–Ge alloy films on the P-type Si(100) substrates. The substrates were pretreated using a standard Radio Corporation of American (RCA) procedure [13] and a 15-s immersion in the solution mixed with HF and H_2O (1:50 in volume ratio). Initially, a 120-nm Si–Ge layer was deposited at 500 °C for 43 min from the mixed atmosphere of SiH_4 (85 sccm) and GeH_4 (15 sccm) maintained at 10^{-7} mbar. Consequently, a

* Corresponding author. Tel./fax: +886 49 2563489x3606.
E-mail address: chtsai12@gmail.com (C.-H. Tsai).
[1] The first and second author contributed equally to this work.

0022-0248/$ - see front matter © 2013 Elsevier B.V. All rights reserved.
http://dx.doi.org/10.1016/j.jcrysgro.2013.12.013

10-nm Si buffer layer was deposited on the Si substrate at 500 °C for 100 min from pure SiH_4 (5 sccm) at 10^{-7} mbar. The SiGe and Si buffer layers were deposited following four cycles till the total thickness of film reached 530 nm. After film fabrication, a composition of films was confirmed as $Si_{80}Ge_{20}$ via an electron probe microanalyzer (EPMA, JEOL JAX-8800). The temperatures of annealing treatments for $Si_{80}Ge_{20}$ films were RT, 800, 900, and 1000 °C for 30 min in argon atmosphere. A nanoindentation measurement system (Hysitron) equipped with atomic force microscopy (AFM, Digital Instruments Nanoscope III) was applied for recording the load–displacement (P–δ) curves of the alloy films. The test strain rate was at 0.05 s^{-1}, and each P–δ curve was repeated at least three times to ensure reproductivity. The surface morphologies of as-synthesized and indented samples were observed using the conjunct AFM. The grazing incidence X-ray diffraction (GIXRD) instrument used was a Shimadzu XRD-6000 with Cu K_α radiation operated at 30 kV and 20 mA. The scanning speed was 1°/min. After the sample preparation by a focus ion beam (FIB), the cross-sectional transmission electron microscopy (TEM) images of a 900 °C-annealed film were recorded using a JEOL JEM-2100F operating at 200 keV.

3. Results and discussion

In order to exclude a measurement error resulting from the excessive surface deviation, AFM was applied to inspect the topological morphology for the samples before the indentation measurement. Fig. 1(a) displays the AFM image for the RT-annealed sample with the root mean square roughness (R_{rms}) value of 37.40 nm. A 3D-curved surface with no abnormal cracks represents the films well grown via the UHV-CVD system. An AFM analysis obtained from the samples is as follows. The R_{rms} values of 800 °C-, 900 °C-, and 1000 °C-annealed films are 35.30, 36.45, and 33.83 nm, respectively. Notice that these R_{rms} values are much smaller than the maximum indentation depth (100 nm). Therefore, one can rule out the extrinsic deviations of mechanical properties which were varied with the surface condition of the sample. Next, we take the RT-annealed film, for example, to represent the closely experimental results for the samples in this study. Fig. 1(b) demonstrates the 2D AFM image for the RT-annealed sample after the indentation test. As observed in the central indentation zone, a regular triangle with no crack, shows that the pressure is uniformly applied on the sample. Fig. 1(c) reveals the load–displacement (P–δ) curves obtained from the nanoindenter. As the repeated curves are well stacked with each other, it implies a good reproductivity of our measurements. As the arrows indicated, h_{max}, h_c, and h_f are the maximum indentation depth, the contact depth, and the final depth, respectively. Herein, the parameters related to the mechanical performance in this article are referred as above. To probe mechanical characteristics in advance, Table 1 lists parameters as revealed by elastic modulus (E), hardness (H), E/H, the final displacement after complete unloading (h_f), the maximum indentation depth (h_{max}), and h_f/h_{max}. One can see that the H value increases with the annealing temperature in the initial stage (from RT to 900 °C), and further decreases with that in the final stage (> 900 °C). Besides the primitive H value, complex parameters including E/H and h_f/h_{max} values yield useful information to elucidate an interior mechanical character of materials. In comparison with H values, both E/H and h_f/h_{max} values appear to have an inverse tendency as a function of annealing temperature (See Fig. 2). The most important difference between E/H and bare H values is that E input to E/H truly specifies the substantial elastic recovery for a material. Owing to the insignificant influence of E, the ratio (E/H) does not vary much for different pure brittle solids [14]. In this study, the E/H values strongly depend on the annealing temperatures. This helps in providing the phase transformation insight into the hard metal matrix after a thermal treatment. Zhou et al. [15] fabricated alloys with the composition of $AlCoCrFeNiTi_x$ (x=0, 0.5, 1.0, 1.5), and gradually increased E values with adding a Ti element. Based on the BCC solid solution lattice, the lattice distortion

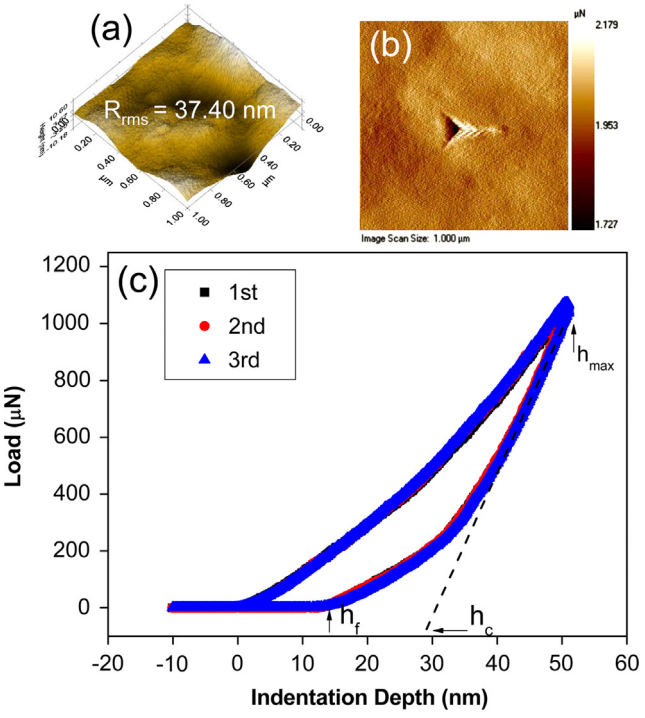

Fig. 1. (a) 3-d AFM image of RT-annealed $Si_{80}Ge_{20}$ alloy films before the indentation, (b) 2-d AFM image of RT-annealed film after the indentation, and (c) the P–δ curves repeated for three times for RT-annealed sample in the depth of 100 nm, where h_c, h_f, and h_{max} are the contact depth, the final depth, and the maximum indentation depth, respectively.

Table 1
Typical mechanical parameters acquired from the P–δ plots of the samples annealed at RT, 800 °C, 900 °C, and 1000 °C, respectively.

Sample condition	E (GPa)	H (GPa)	E/H	h_f (nm)	h_{max} (nm)	h_f/h_{max}
RT annealing	182.5 ± 0.8	12.3 ± 0.2	14.83	13.8	50.8	0.271
800 °C annealing	188.3 ± 0.4	12.9 ± 0.1	14.59	13.3	50.8	0.261
900 °C annealing	190.1 ± 0.7	13.1 ± 0.1	14.51	13.0	50.6	0.256
1000 °C annealing	186.1 ± 0.5	12.5 ± 0.2	14.88	13.5	50.9	0.265

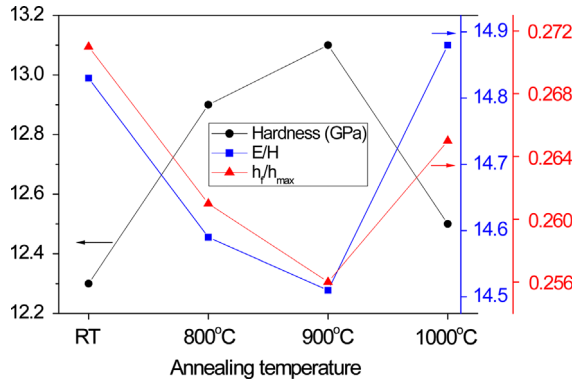

Fig. 2. The temperature-dependent plots of H, E/H, and h_f/h_{max} values for the samples, where H, E, h_f, and h_{max} are the hardness, the elastic modulus, the final displacement after complete unloading, and the maximum indentation depth, respectively.

energy will increase significantly and the solid solution strengthening will be enhanced because a Ti atom, with a larger atomic radius, occupies the lattice sites. Hence, E undoubtedly increases with x in $AlCoCrFeNiTi_x$. Inferred from the Si–Ge phase diagram [16], the incensement of E/H ratio with elevating the annealing temperature from RT to 900 °C can be explained via the same mechanism since $Si_{80}Ge_{20}$ is basically a diamond-like solid solution. However, the mechanism of the descending hardness while temperature surpassing 900 °C needs detailed verification. The h_f/h_{max} acquired from the unloading P–δ curve can be used to clarify the sample in the nanoindentation experiment; the natural limits for the h_f/h_{max} parameter are $0 \le h_f/h_{max} \le 1$, where the lower limit and the upper one correspond to the full elastic deformation and a rigid-plastic behavior [17]. On the basis of $h_f/h_{max} < 0.7$, dominated by the sink-in effect [18], the decreasing of h_f/h_{max} values from RT to 900 °C could be suspected for the solid solution strengthening which is considered as a weak type of hardening. Fig. 3 shows the XRD patterns for the $Si_{80}Ge_{20}$ alloy films after RT-, 800 °C-, 900 °C-, and 1000 °C-annealing treatments, respectively. Three main groups of peaks are locating around 66.6–67.0, 67.8, and 69.2°, corresponding to pure Ge, Si–Ge alloy, and Si substrate, respectively. As the red-dashed line indicated, the peaks are attributed to the Si–Ge(400) plane-shift leftward with the temperatures ranging from RT to 900 °C, and correspondingly show a right shift for temperatures higher than 900 °C. The lattice parameters of RT-, 800 °C-, 900 °C-, and 1000 °C-annealed samples are 5.519, 5.521, 5.524, and 5.515 Å, respectively. It implies that the lattice parameters of the investigated Si–Ge films increase with the temperatures from RT to 900 °C but then reduce with temperatures greater than 900 °C. The expansion of the lattice parameters strongly supports the solid solution strengthening mechanism to cause the hardness increasing that varies with the annealing conditions. The processing of Si–Ge films involves thermal dissociations of SiH_4 and GeH_4 gases. Unavoidably, a small amount of pure elemental Ge or Si exists in the as-synthesized film. The annealing treatment promotes entire mixing of alloying elements, and accompanies the solid solution strengthening effect. Notice that the lattice parameters of Si and Ge are 5.43 [19] and 5.65 Å [20], respectively. The peak shifting leftward signifies increasing of the lattice parameter which warrants dissolving the elemental Ge atoms into the Si-based matrix in the annealing process. Thus rather instead of a pure Si lattice, an enlarged lattice parameter occurs. On the other hand, the over-annealing treatment (> 900 °C) demotes the hardness effect. As the experimental segregation enthalpy of Si–Ge alloy is only 5.3 ± 0.5 kJ mol^{-1} [21], the precipitation of elemental Ge causes the decayed hardness, after Ge atoms get enough thermal energies to overcome the activation barrier. As displayed in Fig. 3, the broaden Ge peak at 900 °C points to the presence of amorphous Ge, while the raised Ge peak at 1000 °C displays the nanoscaled Ge. The precipitation of Ge not only weakens the solid solution strengthening but also creates the right shift of the peak. Fig. 4(a) shows the bright-field (BF) TEM micrograph including the Si substrate, the Si–Ge alloy films, and the ultra-thin silicon buffer layers for the samples after the 900 °C annealing. Fig. 4(b) exhibits the high resolution (HR) lattice image obtained from the blue rectangle marked in Fig. 4(a). As shown in the upper-inset figure, the lattice spacing with the value of 2.812 Å roughly satisfies the spacing of the (200) plane for the Si–Ge alloy. Fig. 4(d) demonstrates the selected area diffraction patterns (SADP) obtained from the region shown in Fig. 4(b). As can be seen, the [1 − 11], [200], [11 − 1] spots from the [110] zone axis confirms existence of the diamond cubic structure. The lattice spacing calculated from the (200), the experimental lattice parameter in Fig. 4(b) is 5.624 Å, evidencing segregation of Ge (Notice

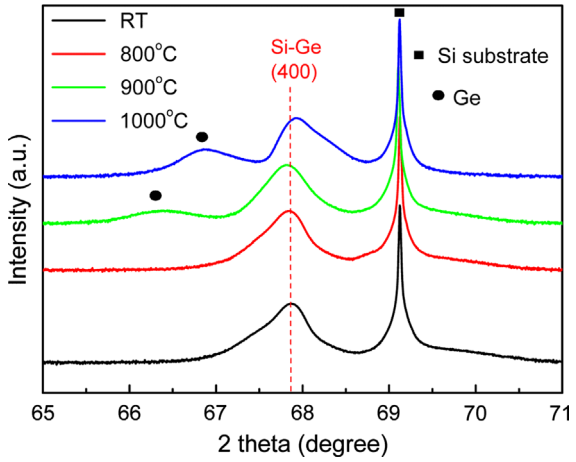

Fig. 3. The GIXRD patterns for the samples annealed at different temperatures.

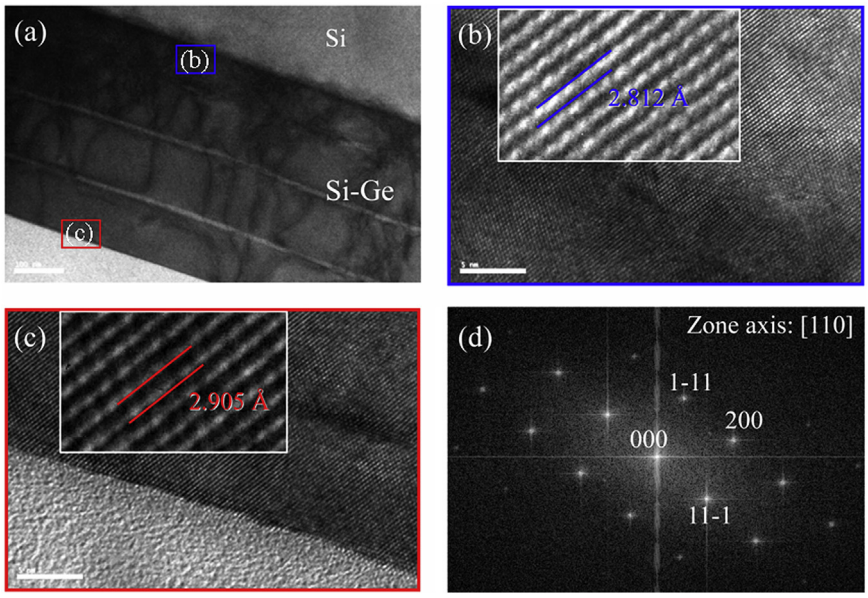

Fig. 4. The cross-sectional TEM morphology of 900 °C annealed film. (a) The bright filed image of the region including the Si substrate, Si–Ge alloy films, and ultra-thin silicon buffer layers. (b) The HR lattice image obtained from the blue rectangle marked in (a). (c) The HR lattice image enlarged from the red rectangle marked in (a). (d) The selected area diffraction patterns (SADP) of (b). (For interpretation of the references to color in this figure legend, the reader is referred to the web version of this article.)

that the lattice parameter of pure Ge is 5.650 Å [20]). This result validates our conjecture that the decreasing hardness is contributed by the Ge cluster once again. In addition, Fig. 4(c) shows the HR lattice image (The upper-inset figure displays in enlarged scale) for the area marked with the red rectangle in Fig. 4(a). Corresponding to the quartz (151) plane, the referred lattice spacing (2.913 Å, JCPDS: 2-471) and the experimental one (2.905 Å) are close to each other. It expresses the presence of SiO_2 on the top layer of the alloy film, even though the sample was annealed in the Ar atmosphere.

4. Conclusion

This study investigates the mechanical performances of $Si_{80}Ge_{20}$ alloy films annealed at RT, 800 °C, 900 °C, and 1000 °C, respectively. The samples were indented in the depth of 100 nm to probe the intrinsic mechanical properties in avoidance of the extrinsic disturbances including the abnormal crack and the excess deviation of roughness. Recorded from the load–displacement curves, the hardness value increases with the annealing temperature ascended from RT to 900 °C, and further deceases with that elevated higher than 900 °C. Accordingly, both E/H and h_f/h_{max} values appearing an inverse tendency in the above temperature range hints the occurrence of the solid solution strengthening, and implies a soft phase segregating at a temperature higher than 900 °C. Meanwhile, XRD analysis demonstrates that the lattice expansion and the broadened peak attribute to the solid solution strengthening of $Si_{80}Ge_{20}$ and the segregation of Ge, respectively. Expected as a symptom of the abruptly descended hardness for 1000 °C-annealed sample, TEM analysis evidences the segregation of Ge for the 900 °C-annealed one in the presence of the (200) lattice spacing of 5.624 Å.

Acknowledgments

The authors thank Prof. C.P. Chou for technical support (Department of Mechanical Engineering, National Chiao Tung University). We also thank Dr. H.C. Wen and Prof. W.C. Chou for technical suggestions, and Prof. Y.R. Jeng for the SPM equipmentused in this study.

References

[1] Y. Yukimoto, M. Aiga, a-SiGe:H alloy and its application to tandem-type solar cell, in: MRS Online Proceedings Library, 70, 1986.
[2] F.Y. Huang, X. Zhu, M.O. Tanner, K.L. Wang, Normal-incidence strained-layer superlattice $Ge_{0.5}Si_{0.5}$/Si photodiodes near 1.3 μm, Appl. Phys. Lett. 67 (1995) 566–568.
[3] T. Yoshida, Y. Yamada, N. Suzuki, T. Makino, T. Orii, K. Murakami, D. Geohegan, D.H. Lowndes, M.J. Aziz, Crystallinities and light- emitting properties of nanostructured SiGe alloy prepared by pulsed laser ablation in inert background gases, Proceedings of SPIE 3618 (1999) 512–519.
[4] B. Schuppert, J. Schmidtchen, A. Splett, U. Fischer, T. Zinke, R. Moosburger, K. Petermann, Integrated optics in silicon and SiGe-heterostructures, J. Lightwave Technol. 14 (1996) 2311–2323.
[5] SiGe: a key to unlocking the potential of solar cells, Photovoltaics Bulletin, 2003, pp. 7–9.
[6] S.S. Iyer, G.L. Patton, J.M.C. Stork, B.S. Meyerson, D.L. Harame, Heterojunction bipolar transistors using Si–Ge alloys, IEEE Trans. Electron Devices 36 (1989) 2043–2064.
[7] Y. Wu, R. Fan, P. Yang, Block-by-block growth of single-crystalline Si/SiGe superlattice nanowires, Nano Lett. 2 (2002) 83–86.
[8] J.A. Babcock, P. Francis, R. Bashir, A.E. Kabir, D.K. Schroder, M.S.L. Lee, T. Dhayagude, W. Yindeepol, S.J. Prasad, A. Kalnitsky, M.E. Thomas, H. Haggag, K. Egan, A. Bergemont, P. Jansen, Precision electrical trimming of very low TCR poly-SiGe resistors, Electron Device Lett., IEEE 21 (2000) 283–285.
[9] V. Subramanian, M. Toita, N.R. Ibrahim, S.J. Souri, K.C. Saraswat, Low-leakage germanium-seeded laterally-crystallized single-grain 100-nm TFTs for vertical integration applications, Electron Device Lett., IEEE 20 (1999) 341–343.
[10] P. Kringhøj, R.G. Elliman, J.L. Hansen, The effect of strain and strain-gradients on the crystallisation kinetics of $S_{1-x}Ge_x$ Alloy Layers, in: MRS Online Proceedings Library, 321, 1993.
[11] D. Parnis, E. Zolotoyabko, W.D. Kaplan, M. Eizenberg, N. Mosleh, F. Meyer, C. Schwebel, Structural disorder in SiGe films grown epitaxially on Si by ion beam sputter deposition, Thin Solid Films 294 (1997) 64–68.
[12] K.L. Whiteaker, I.K. Robinson, J.E. Van Nostrand, D.G. Cahill, Compositional ordering in SiGe alloy thin films, Phys. Rev. B 57 (1998) 12410–12420.
[13] H.-W. Liu, W.-K. Lai, S.-Y. Yu, S.C. Huang, H.-C. Cheng, Materials science communication effects of rca clean-up procedures on the formation of roughened poly-si electrodes for high-density drams′ capacitors, Mater. Chem. Phys. 51 (1997) 195–198.
[14] B. Basu, M. Kalin, Tribology of Ceramics and Composites: Materials Science PerspectiveThe American Ceramic Society, Wiley, 2011 522 pp.
[15] Y.J. Zhou, Y. Zhang, Y.L. Wang, G.L. Chen, Solid solution alloys of $AlCoCrFeNiTi_x$ with excellent room-temperature mechanical properties, Appl. Phys. Lett. 90 (2007) 181904-1–181904-3.
[16] R.W. Olesinski, G.J. Abbaschian, The Ge–Si (Germanium–Silicon) system, Bull.. Alloy Phase Diagr. 5 (1984) 180–183.
[17] W.C. Oliver, G.M. Pharr, Measurement of hardness and elastic modulus by instrumented indentation: advances in understanding and refinements to methodology, J. Mater. Res. 19 (2004) 3–20.
[18] P. Waters, U.o.S. Florida, Stress Analysis and Mechanical Characterization of Thin Films for Microelectronics and MEMS ApplicationsUniversity of South Florida, 2008 http://gradworks.umi.com/33/47/3347380.html.
[19] W.L. Bond, W. Kaiser, Interstitial versus substitutional oxygen in silicon, J. Phys. Chem. Solids 16 (1960) 44–45.
[20] S.B. Qadri, E.F. Skelton, A.W. Webb, High pressure studies of Ge using synchrotron radiation, J. Appl. Phys. 54 (1983) 3609–3611.
[21] J. Nyéki, C. Girardeaux, G. Erdélyi, A. Rolland, J. Bernardini, Equilibrium surface segregation enthalpy of Ge in concentrated amorphous SiGe alloys, Appl. Surf. Sci. 212–213 (2003) 244–248.